Characterization of organic content, brittleness index and geomechanical properties of the Eocene Cambay Shales – Insights from the Ankleshwar oil field in Western India

Article *in* Interpretation · November 2020

DOI: 10.1190/int-2020-0133.1

CITATIONS
0

READS
119

3 authors:

Shib Sankar Ganguli
National Geophysical Research Institute
43 PUBLICATIONS **128** CITATIONS
SEE PROFILE

Souvik Sen
Geologix Limited
46 PUBLICATIONS **299** CITATIONS
SEE PROFILE

Sumit Verma
University of Texas of the Permian Basin
70 PUBLICATIONS **191** CITATIONS
SEE PROFILE

Characterization of organic content, brittleness index, and geomechanical properties of the Eocene Cambay Shales — Insights from the Ankleshwar oil field in western India

Shib Sankar Ganguli[1], Souvik Sen[2], and Sumit Verma[3]

Abstract

Shale resource assessment involves a detailed characterization of organic and geomechanical parameters for better insights on the reservoir properties and classifying areas of economic yield. To assess the Eocene Younger Cambay Shale (YCS) Group of the Ankleshwar field, western India, for feasible shale resource play, we have applied a multistage screening methodology that combines an estimation of organic richness, brittleness index (BI), and geomechanical analyses. The estimated thermal maturity and average total-organic-carbon (TOC) contents are within the range of 0.8–1.0 and 1.8 wt%, respectively. These estimates are comparable to the reported core-based measurements. BI based on the mineralogical composition reveals that the YCS intervals of marine origin fall into the "less-ductile" to "brittle" zone, whereas the elastic property-based estimated BI falls into the "less-brittle" to "high brittle" zone. We have established a field relationship between the BI and the shale volume, and we also deciphered the effect of TOC content on the rock-elastic properties. Pore pressure in the shales is slightly above the hydrostatic gradient (10.5–11.5 MPa/km). The estimated average fracture pressure of 18.5 MPa/km, together with the BI of moderately ductile to less-brittle behavior suggests that the studied shales are capable of withstanding substantial strain while hydrofracturing for effective production. We demonstrate an expedient example to characterize a potential shale unit within a producing hydrocarbon field using the drilled wells with limited or no core data.

Introduction

The depletion of existing conventional oilfields globally has critical implications in the unconventional exploration strategy. Over the past decade, shale-gas/oil development has emerged as a proven unconventional energy resource due to its huge success (Bakshi et al., 2017; Ghazwani et al., 2018; Liu et al., 2018; Wang et al., 2018), especially in the west. The surging shale-gas production in the Western Hemisphere and the potential of replicating the same success worldwide can significantly revolutionize the global energy scenario. Some argue that shale-gas/oil resource has already been ascertained as a game changer in the U.S. and Canadian energy market (Soeder, 2018). India, being the most significant importer and consumer of hydrocarbon resources, shows great interest in domestic shale-gas exploration and production to meet the quest for energy. In a scenario such as this, evaluation of potential national unconventional resources becomes crucial, and, if successful, it may not only strengthen the Indian national hydrocarbon resource volume, but it also may attract foreign investment. Until now, proven conventional resources had been the primary exploration and development target in the Cambay Basin. Nevertheless, with enduring energy demand, growing interest in unconventional resources, and due to substantial capacity of shale-gas/oil potential of the Younger Cambay Shale (YCS) Group just beneath the Ankleshwar Formation, this basin has been given special attention for a detailed evaluation of essential and desirable shale resource play parameters. Moreover, the successful hydrofracturing in this basin (Sharma et al., 2010) unlocked new hope and frontiers for a comprehensive investigation into shale-gas exploration and development in India.

Hydrocarbon generation depends directly on the burial depth, temperature, and organic matter type of the rock (Rasmussen, 2005). Buried sediments are subjected to increased temperature (due to the subsurface temperature gradient) and pressure (due to the weight of the overburden), resulting in compaction

[1]CSIR-National Geophysical Research Institute, Uppal Road, Hyderabad 500007, Telangana State, India. E-mail: shibg@ngri.res.in (corresponding author).
[2]Geologix Ltd., Dynasty Building, Andheri Kurla Road, Andheri East, Mumbai 400059, Maharashtra, India. E-mail: souvikseniitb@gmail.com.
[3]University of Texas Permian Basin, 4901 East University Blvd., Odessa, Texas 79762, USA. E-mail: verma_s@utpb.edu.

Manuscript received by the Editor 24 June 2020; revised manuscript received 25 September 2020; published ahead of production 11 November 2020; published online 20 January 2021. This paper appears in *Interpretation*, Vol. 9, No. 1 (February 2021); p. T235–T252, 16 FIGS., 6 TABLES.
http://dx.doi.org/10.1190/INT-2020-0133.1.

DOI:10.1190/INT-2020-0133.1

and diagenesis. Organic constituents of sedimentary rock, that is, kerogen converted into oil/gas during catagenesis and cracked during metagenesis. Hydrocarbon production from the low-porosity and -permeability shale reservoirs is a difficult task due to their variable lithologic characteristics (Yang et al., 2019), and special care should be taken while characterizing such rocks (Busch and Amann-Hildenbrand, 2013). For a successful shale resource play assessment, more attention is needed on shale characteristics such as total-organic-carbon (TOC) content (organic richness), thermal maturation, mineralogical composition, and geomechanical properties, unlike conventional reservoir characterization, in which the focus is mainly directed towards estimation of reservoir properties. An optimum amalgamation of the parameters such as organic richness and geomechanical properties is an indispensable factor that led to favorable productivity in shale formations. Organic richness (mid to high kerogen content), lesser clay volume, higher Young's modulus, lower Poisson's ratio, and high brittleness index (BI) characterize the sweet spots for ideal shale-gas reservoirs (Kenomore et al., 2017). Sweet spots are the areas of a shale play with the most essential and desirable properties and increase the success of stimulation processes, that is, hydraulic fracturing and hence production potential.

Despite several hydrocarbon exploration and geochemical studies in the Cambay Basin, western India (Biswas et al., 2013; Mishra et al., 2014; Ganguli et al., 2016a, 2016b, 2017, 2018; Ganguli, 2017; Jaiswal and Bhattacharya, 2018), very few studies have been reported to comprehend the shale-gas/oil reserves and development potential through geophysical and fracture development studies (Sharma et al., 2010; Ariketi et al., 2017b). The present hydrocarbon exploration licensing policy of India has enabled the operators to exploit conventional as well as unconventional resources together from a single hydrocarbon license. Ankleshwar field is one of the most productive fields in the Cambay Basin, which is now witnessing the declining phase of production (Ganguli et al., 2016a, 2016b; Ganguli, 2017). Hence, development infill wells are usually being drilled to maintain production. These wells have penetrated and encountered a good interval of the YCS Formation almost everywhere, which provides a unique opportunity to investigate the YCS intervals for its unconventional resource potential in the same wells apart from exploiting the primary conventional target (the Ankleshwar Formation). The main objective of this work is to characterize the shale-gas parameters/factors of the YCS in the Cambay Basin and discuss its implications for potential resource evaluation. To do so, we need to adopt a multistage comprehensive screening methodology, including measurement of thermal maturity and TOC content and estimation of geomechanical parameters such as the stress components, pore pressure (PP), and BI of the YCS Formation from the studied field. To estimate BI, rock minerology and elastic property-based approaches have been used in the present study. We assess the Ankleshwar oil field in the Cambay Basin for the first time for its shale-oil/gas production potential through the analysis of geophysical, geomechanical, and other relevant properties, intending to transform geophysical facts into shale fracture development and its resource potential.

Geologic setting of the area

The Cambay Basin is an elongated (approximately 425 km long) intracratonic rift graben trending north-northwest–south-southeast, located in western India, covering an area of approximately 55,000 km^2. The Cambay rifting took place after the episodic Deccan volcanism approximately 65 Ma that resulted in basin bounding extensional fault system, which largely consists of two types of faults, that is, "listric normal faults" and "transfer faults," along the preexisting basement. It is believed that the sedimentation in this petroliferous basin is predominantly controlled by prerift, synrift, and postrift phases. The tectonic deformation in this basin is reasonably deep, which leads to various graben or half-graben structures. The unconformable relation between the Olpad Formation and the underlying Cambay Shale indicates two major phases of extension in this basin. Thermal subsidence initiated during the Mid Eocene, which was incessant for a while until the Early Miocene (Banerjee et al., 2000). Data from burial history suggest that hydrocarbon generation in this basin occurred during the Miocene and Early Pliocene, which migrated vertically mainly along faults to form the reservoir. Burial depths are not much deeper, and source rocks are believed to be more mature in the deepest part of the western offshore region of India (Biswas et al., 2013). Temperature and time are two most important factors that control the hydrocarbon generation in any basin. The thermal history of this basin indicates an initial high heat flow regime, which was later followed by a basin-wide cooling phenomenon that helped in the generation and preservation of hydrocarbon resources in the basin. A more detailed study on the thermal regime, temperature distribution, and the origin of the basin has been reported by Ganguli et al. (2018).

The occurrence of hydrocarbons in this basin ranges from the Paleocene through Miocene, including the key accumulations in the Middle Eocene, which are due to various structural traps linked with block uplifts and edge folds. Oil and gas in the Ankleshwar field are primarily produced from deltaic depositions. This hydrocarbon-bearing field covers an area of approximately 32 km^2 (Ganguli, 2017). Figure 1 depicts the present study area within the Cambay Basin. The stratigraphic section of the Ankleshwar oil field is well-developed and consists of a thick Tertiary sedimentary pile aged Eocene–Pliocene, overlying the Deccan basalts of Cretaceous age (Mukherjee, 1981; Ganguli et al., 2019). The regional stratigraphy of the Ankleshwar field is presented in Table 1.

The Cambay Shale is a proven source rock of excellent quality and is responsible for hydrocarbon

DOI:10.1190/INT-2020-0133.1

generation in the basin. A major transgressive event (marginal marine) during the Early Eocene has deposited the thick (approximately 220–470 m) Cambay Shale sequence. Petrographic analysis suggests that the Cambay Shale sequence comprises a lithology dominated by tight and moderately laminated carbonaceous shale with a clay-rich matrix (Kumar et al., 2017). Most of the shale samples are not cemented, and comparatively deeper shales are more cemented than the younger shales (Ganguli et al., 2016b). The dominant shale units of the Cambay Basin are the Olpad Formation (Paleocene), Older Cambay Shale (OCS) Formation (Paleocene-Early part of the Lower Eocene), YCS Formation (Lower Eocene), Kalol/Ankleshwar Formation (Mid Eocene to Upper Eocene), and Tarapur Formation (Upper Eocene to Oligocene). In general, the Older Cambay Shale is gray to dark gray, moderately fissile, and comprises occasional siltstone. On the other hand, the YCS member is gray to black, massive sideritic, and carbonaceous (occasionally calcareous) in nature. The mineralogical composition of the Ankleshwar region is mainly quartz, with an average value of 54.53%, as presented in Figure 2. Following these are clay minerals, with an average content of 27.22%. The calcite minerals are the lowest, with content of less than 10%. The Cambay Shale mineralogical data set is plotted on the sCore mineralogy ternary diagram depicting how well the studied shale compare with that of the North American (e.g., Barnett, Fayetteville, Marcellus, Haynesville, and Eagle Ford) and UK (Kirby Misperton) unconventional plays (Figure 2).

The Cambay Shale sequence is present in all of the major tectonic depressions covering the Upper Paleocene to Middle Eocene age. Figure 3 shows a schematic seismogeologic cross section of the basin that includes key faults systems, facies variation, and well locations emphasizing the Ankleshwar oil field along

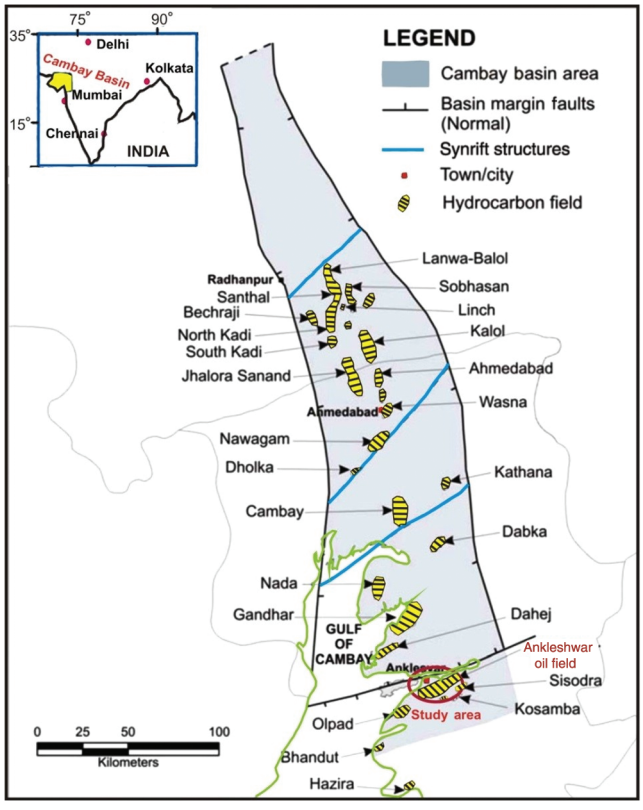

Figure 1. The Ankleshwar oil field (marked by a red ellipse) within the Cambay Basin, along with major basin bounding faults, synrift structures, and other proven hydrocarbon fields (adapted from Ganguli et al., 2016a).

Table 1. Regional stratigraphic column of the Ankleshwar field at the Cambay Basin, the study area.

Age	Formation and thickness
Recent	Gujarat Alluvium (15–40 m)
Pleistocene	Jambusar Formation (100–300 m)
Pliocene	Broach Formation (~300 m)
Miocene	Jhagadia Formation (~200 m)
	Kand Formation (~200 m)
	Babaguru Formation (125–300 m)
Oligocene	Dadhar Formation (90–145 m)
Eocene	Ankleshwar Formation (300–400 m)
	Cambay Shale Group (220–470 m)
Palaeocene	Olpad Formation (20–200 m)
Cretaceous	Deccan Trap (324+ m)
	Seru Formation
Archean	Granitic Basement

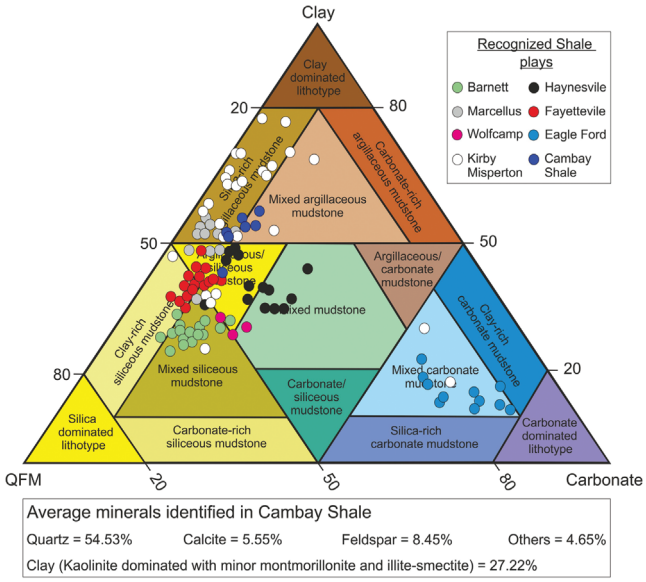

Figure 2. An sCore mineralogy ternary diagram with superimposed mineralogical composition (%) from the studied shale samples, modified after Glaser et al. (2014). For comparison, the mineralogical compositions of the Eocene Cambay Shales are plotted together with the major North American and Kirby Misperton, UK, shale plays.

the northeast and southwest directions. After the deposition of organic-rich Cambay Shale, a regressive phase prevailed during the Middle Eocene to the Upper Eocene, which deposited the Ankleshwar Formation on top of the Cambay Shale Group. The oil generation and migration attain a peak during the Early to Middle Miocene. Hazad and Ardol subunits of the Middle to Upper Eocene within the Ankleshwar Formation are the key pay zones of deltaic origin.

Data

In this study, wireline log data, well completion reports, and summaries from four exploration vertical wells drilled in the Ankleshwar field, together with the mudlogging data set (surface drilling parameters and mud weight) and various downhole measurements (formation pressure and leak-off test [LOT]), were used. The high-resolution wireline log suite comprises gamma-ray, deep resistivity, formation density, and sonic slowness, which were useful in conducting this study. Figure 4 portrays the well-to-well correlation used to understand the stratigraphic variation and delineate the target formation interval in all of the wells, as presented in Table 2. The YCS exhibits high gamma-ray values in all well logs, which was used as a primary factor for the well-log correlation. Overall, the top of the YCS Formation is characterized by clean shale, whereas intercalations of thin sandstone/siltstones were observed at the bottom part, especially in wells W-13 and W-14, respectively. The maximum thickness of 180 m was found in well W-12, whereas W-14 exhibits a minimum thickness of 130 m. The overall 100 m+ thickness of the targeted YCS Formation in all four wells was the key factor for being selected for this study. Apart from these available data, published core data were used to corroborate our results and interpretations.

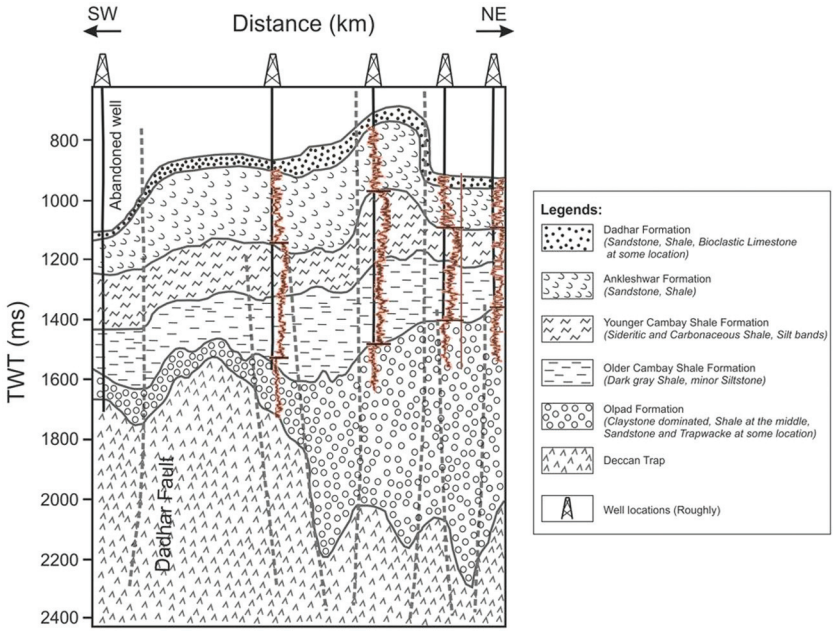

Figure 3. Schematic representation of the northeast–southwest seismogeologic cross section of the Ankleshwar block located in the Cambay Basin with the approximate location of the drilled wells (after Ganguli and Sen, 2020). The log overlayed here is gamma-ray log as obtained from the studied wells.

Analytic methods

Thermal maturity and TOC

The thermal maturity (R_o) is a critical parameter for the unconventional resource play, and it translates to the maximum temperature that a rock has attained during burial over the geologic period. Rock-Eval T_{max} is also commonly used to estimate R_o (Jarvie et al., 2001), as given in the form

$$T_{max}\ \text{eq\%R}_o = 0.018(T_{max}) - 7.16, \quad (1)$$

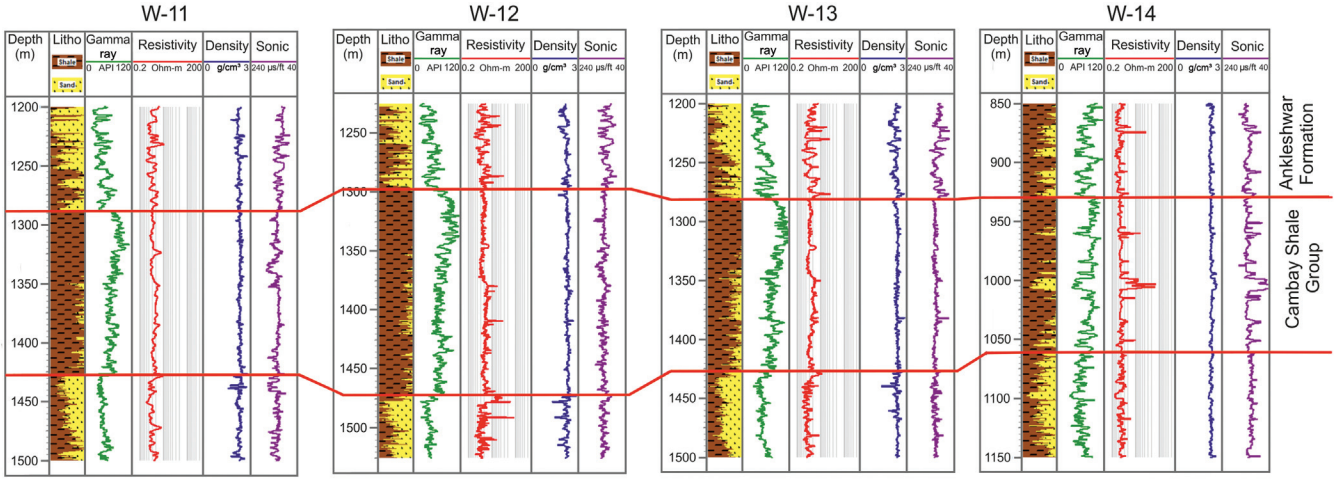

Figure 4. Representation of the YCS Formation as correlated among the four wells from the Ankleshwar field, the study area.

where T_{max} eq% R_o is the thermal maturity in which the Rock-Eval T_{max} value is converted into a vitrinite reflectance equivalent value. Mallick and Raju (1995) establish a mathematical best-fitting relationship between Ro and the interval transit time from Tertiary sediments of the Upper Assam Basin. In a recent study, Tyagi et al. (2011) establish the following relationship between the sonic log and vitrinite reflectance from direct measurements in the wells from the Cambay Basin:

$$R_o = (353.51 - \Delta t\mathrm{CO})/441.83, \quad (2)$$

where ΔtCO = the compressional sonic log in μs/ft unit. Because these direct core-based measurements were unavailable from the studied wells, we used equation 2 to estimate R_o in our study area.

The organic matter present within a source rock is called the total organic content (TOC) and is measured in wt% units. The fluid produced or found in a source rock depends on the type of organic matter. Accurate estimation of TOC is vital for the evaluation of shale-gas reservoirs. TOC and R_o together characterize whether a rock is a good source rock or not. In this study, we have used two methods to estimate the TOC. The first one is Passey's method (Passey et al., 1990), a widely used tool, which has been used to calculate TOC across the shale intervals. This method uses the responses of the resistivity log and sonic log to organic matter, which is useful in the scarcity of the core data (Verma et al., 2016). Overlay of resistivity and sonic log produces a separation against an organic-rich interval, termed as delta LogR (ΔLog R). Low-density kerogens affect the response of the porosity curve, and the resistivity curve responds to the formation fluid; hence, an overlay of both curves produces the mentioned separation (Passey et al., 1990). The equation to calculate ΔLog R is as follows:

$$\Delta\mathrm{Log\,R} = \log_{10}\left(\frac{\mathrm{R}}{\mathrm{Rbase}}\right) + 0.02 * (\Delta t - \Delta t\mathrm{base}), \quad (3)$$

where R is the deep resistivity (ohm-m) and Δt is the compressional sonic slowness (μs/ft). The terms Rbase and Δtbase are the baseline resistivity and traveltime values, respectively, in non-source-rock intervals. TOC can be estimated knowing the ΔLog R and the level of organic maturity (LOM) because ΔLog R is proportional to TOC and LOM. In addition, LOM is dependent on Ro and can be calculated using the following equation:

$$\mathrm{LOM} = (0.0989 * {R_o}^5) - (2.1587 * {R_o}^4) + (12.392 * {R_o}^3) - (29.032 * {R_o}^2) + (32.53 * R_o) - 3.0338. \quad (4)$$

Finally, the TOC along the depth intervals can be estimated using Passey's equation, as given below:

$$\mathrm{TOC} = (\Delta\mathrm{Log\,R}) * 10^{2.297 - 0.1688 * \mathrm{LOM}}, \quad (5)$$

It is worth mentioning that before applying Passey's method to estimate TOC, one should be very careful about the possible presence of pyrites in shale. Pyrites, being conductive, can lower the resistivity reading, thus resulting in reduced ΔLog R, which can yield underestimated TOC values. However, pyrites are absent in the studied shale intervals across the four wells, as seen in the density log responses (pyrites usually possess very high density of approximately 5 g/cm^3).

The second method of TOC estimation used here is based on density, and the equation is as below (Vernik and Landis, 1996; Carcione, 2000):

$$\mathrm{TOC} = \frac{\mathrm{a}[\rho_k(\rho_m - \rho_b)]}{[\rho_b(\rho_m - \rho_k)]}. \quad (6)$$

where ρ_k is the kerogen density, which usually varies between 1.1 and 1.6 g/cm^3 (Vernik and Milovac, 2011; Dang et al., 2016; Hansen et al., 2019). We have assumed a kerogen density of 1.1 g/cm^3. The term ρ_m is the matrix density = 2.65 g/cm^3, and ρ_b is the bulk-density log. Here, "a" is the constant related to the fraction of organic carbon (Rahman et al., 2020). We have used a = 67, as suggested by Vernik and Landis (1996).

Estimation of BI

With the increase in stress, rocks undergo three successive deformational stages, namely, elastic, ductile, and brittle. A rock is called brittle if it shows a greater area of elastic response concerning the ductile response. To determine the BI of the targeted Cambay Shale intervals, we used methods that involve the elastic properties and the mineralogical composition as described below.

BI based on the elastic properties

BI can be estimated using dynamic and static elastic properties. In general, the dynamic properties are measured from the compressional sonic wave velocity (V_P) and shear wave velocity (V_S). In the absence of measured V_S data from the studied wells, V_S was estimated following four of the most widely used relationships/models between V_P and V_S. This is to realize a range of variations in the estimated V_S within the studied horizon, which can eventually help to avoid miscalculation in the absence of measured V_S data. Further, rock-physics template (RPT) analyses were conducted to compare the performance of various V_S models for the

Table 2. Correlated depth intervals together with the thickness of the YCS in the studied wells.

Well no.	YCS Formation interval (m)	Thickness (m)
W-11	1280–1425	145
W-12	1295–1475	180
W-13	1280–1425	145
W-14	930–1060	130

DOI:10.1190/INT-2020-0133.1

studied shales. The first model under consideration was established by Castagna et al. (1985):

$$V_P = 1.16V_S + 1.36. \quad (7)$$

The second model was suggested by Han (1986) with km/s as velocity units, which is given below:

$$V_S = 0.794V_P + 0.797. \quad (8)$$

The third and fourth models were established by Greenberg and Castagna (1992) and Nooraiepour et al. (2017a). These two models basically follow the general form of the Castagna et al. (1985) relationship and are modified for multimineral brine-saturated shales as well as mechanically compacted shales, respectively. The relationships are as follows:

$$V_P = 1.3V_S + 1126.88, \quad (9)$$

$$V_P = 1.3V_S + 1172. \quad (10)$$

Table 3 summarizes the equations and parameters that were used to estimate BI based on the elastic moduli.

BI based on mineralogical composition

The general expression of mineralogy-based BI calculation is as follows (Nooraiepour et al., 2017a):

$$BI_{Min} = \frac{F_{SB}}{F_{SB} + F_{WD}}, \quad (11)$$

where BI_{Min} is the brittleness index estimated from mineral composition, F_{SB} is the fraction of strong brittle minerals, and F_{WD} denotes the weak ductile mineral fraction. Various workers have proposed different mineral assemblages under brittle and ductile categories to model the brittleness, which are used in this study and are summarized in Table 4.

Estimation of in situ stress and PP

Understanding of PP and stress tensors is very important in the planning and execution of a reservoir development drilling (Sen et al., 2017, 2018, 2019). The methods for estimation of three stress components, that is, vertical stress (Sv), maximum horizontal stress (SH_{Max}) and minimum horizontal stress (Sh_{min}), and PP in the studied shale intervals have been discussed below.

Table 3. Published relationships/models used to estimate the BIs based on the elastic moduli.

Equation and models	Parameters	Remarks
$BI = \frac{1}{2}\left[\frac{E-E\,min}{E\,max-E\,min} + \frac{\nu-\nu\,min}{\nu\,max-\nu\,min}\right] * 100$	$E = \rho V_S^2\left[\frac{3V_P^2-4V_S^2}{V_P^2-V_S^2}\right]$ $\nu = \frac{V_P^2-2V_S^2}{2(V_P^2-V_S^2)}$ Sone and Zoback (2013)	E = Young's modulus (dynamic elastic property) ν = Poisson's ratio (dynamic elastic property) ρ = formation density Vshale is estimated following the Clavier equation: $\nu_{sh} = 1.7 - \sqrt{(3.38 - (GR_I + 0.7)^2)}$ where $GR_I = \frac{(GR_{log}-GR_{mat})}{(GR_{Shale}-GR_{mat})}$
Model 1: Grieser and Bray (2007)	Dynamic elastic moduli E max = 16 GPA E min = 1.5 GPA ν max = 0.48 and ν min = 0.15	BI = 1 (perfectly brittle) = 0 (perfectly ductile)
Model 2: Rickman et al. (2008)	Static elastic moduli E max = 14.5 GPA E min = 1.5 GPA νx = 0.48 and ν min = 0.15	Correlation between the static and dynamic properties obtained following Mullen et al. (2007): $\nu_{static} = \nu_{dyn}$ $E_{static}[Mpsi] = E_{dyn} * (0.8 - \phi)$, where ϕ = total porosity
Model 3: Guo et al. (2012) $BI = E/\nu$	E = Young's modulus ν = Poisson's ratio	high BI = brittle low BI = ductile

DOI:10.1190/INT-2020-0133.1

The Sv magnitude

The Sv at a particular depth is equivalent to the pressure applied by the overburden litho column. This is also known as overburden stress. Plumb et al. (1991) provide the following equation to estimate Sv from the density logs:

$$\mathrm{Sv} = \int_0^Z \rho(Z) * \mathrm{g}dZ, \tag{12}$$

where Sv = overburden stress/vertical stress, $\rho(Z)$ = formation bulk density at depth Z (available from the wireline density log), and g (i.e., gravitational acceleration) is a constant. Density, being recorded by a padded tool, can provide incorrect and unreliable information against washed-out zones. We explored for enlarged borehole sections in the caliper logs; accordingly, the bulk-density logs were corrected to nullify uncertainties in Sv estimation.

The PP magnitude

Fluids stored in rock's pore spaces exert pressure, which is commonly known as PP. Knowledge of the PP magnitude is crucial for drilling designs (mud, casings, etc.) and for the evaluation of the $\mathrm{Sh_{min}}$ and $\mathrm{SH_{Max}}$ magnitudes (Tingay, 2015; Radwan and Sen, 2020). Eaton (1975) provide the following two expressions to estimate PP using resistivity and compressional sonic slowness logs:

$$\mathrm{PP} = \mathrm{Sv} - (\mathrm{Sv} - \mathrm{P}_h) * \left(\frac{\Delta tn}{\Delta t}\right)^3, \tag{13}$$

$$\mathrm{PP} = \mathrm{Sv} - (\mathrm{Sv} - \mathrm{P}_h) * \left(\frac{\mathrm{R}}{\mathrm{Rn}}\right)^{1.2}, \tag{14}$$

where P_h, Δt, and Δtn are the hydrostatic pressure, the compressional sonic slowness (μs/ft) against the entire interval, and that against normally compacted shales, and R and Rn are the formation resistivity (ohm-m) against the entire interval and that within the normally compacted shale intervals, respectively. In general, normal compaction trend lines (NCTs) are used against the shales (as identified from the gamma-ray log, shale volume logs, and lithology/drill cuttings information) on resistivity and sonic logs to understand and quantify the deviation of the encountered shale intervals from the normally compacted shales. As a common and standard drilling practice, formations are drilled with sufficient mud overbalance; that is, the mud weight is more than the PP to nullify the chances of any kick or fluid influx (Sen et al., 2019, 2020). Therefore, the mud weight can also be used as a representative of the PP upper bound, especially in the absence of logging while drilling logs and wireline logs.

The Sh_{min} magnitude

The $\mathrm{Sh_{min}}$ offers the pressure limit that fractures the formation. The well-known Matthews and Kelly's equation (Matthews and Kelly, 1967), which introduces the effective stress coefficient ($\mathrm{K_e}$), has been used to estimate the fracture pressure in the following form:

$$\mathrm{FP} = \mathrm{PP} + \mathrm{K_e} * (\mathrm{Sv} - \mathrm{PP}). \tag{15}$$

The estimated fracture pressure was calibrated with the LOT data to validate the output. LOT was performed by the operator at multiple casing shoe depths in the studied wells. It represents the maximum allowable mud weight for successfully drilling the section. LOT, being the direct downhole measurement, is the most reliable parameter to calibrate the fracture pressure.

The SH_{Max} magnitude

The $\mathrm{SH_{Max}}$ is not directly measurable within a borehole. Yet, Rajabi et al. (2016) provide an approach to calculate the $\mathrm{SH_{Max}}$ magnitude from the extended LOT (i.e., XLOT). XLOT provides the fracture closure pressure (FCp), which could be used to evaluate the $\mathrm{SH_{Max}}$ using the following equation:

$$\mathrm{SH_{Max}} = 3\mathrm{FCp} - \mathrm{Pr} - \mathrm{PP}, \tag{16}$$

where Pr is the mud pressure during fracture initiation.

Effective stresses

The effective vertical stress ($\mathrm{S_{ev}}$) has been estimated using the equation below:

Table 4. Summary of models used in this study to estimate BI based on mineralogy.

Equation and models	Parameters	Remarks
Model 1: Jarvie et al. (2007)	$F_{\mathrm{SB}} = F_{\mathrm{Quartz}}$ $F_{\mathrm{WD}} = F_{\mathrm{Clay+Carbonate}}$	high $\mathrm{BI_{Min}}$ = brittle low $\mathrm{BI_{Min}}$ = ductile
Model 2: Wang and Gale (2009)	$F_{\mathrm{SB}} = F_{\mathrm{Quartz+Dolomite}}$ $F_{\mathrm{WD}} = F_{\mathrm{Clay+Carbonate+TOC}}$	F_{SB} = fraction of strong or brittle minerals
Model 3: Glorioso and Rattia (2012)	$F_{\mathrm{SB}} = F_{\mathrm{Quartz+Carbonate}}$ $F_{\mathrm{WD}} = F_{\mathrm{Clay+TOC}}$	F_{WD} = fraction of weak or ductile minerals
Model 4: Jin et al. (2014)	$F_{\mathrm{SB}} = F_{\mathrm{Quartz+Carbonate+Feldspar+Mica}}$ $F_{\mathrm{WD}} = F_{\mathrm{Total}} - F_{\mathrm{SB}}$	

$$S_{ev} = Sv - PP. \quad (17)$$

To estimate the effective horizontal stress (S_{eh}), the following equation, which requires the knowledge of Poisson's ratio (ν), has been used

$$S_{eh} = \left(\frac{\nu}{1-\nu}\right) Sv. \quad (18)$$

Results and discussion

Organic content assessment

Core data provide the best and most direct estimate for the TOC and organic maturity of source rocks and hence unconventional resource characterization. The best practice is to estimate the rock properties from geophysical logs and calibrate the log-based outputs with core-based measurements. But coring is a costly and time-consuming operation that is usually carried out in the exploratory phases. The scarcity of core data is a common issue faced in many petroleum interpretation workflows. Hence, to calculate the TOC of the source rock, Passey's method is used and is found to be useful in most successful studies (Verma et al., 2016). In this work, we have studied the already drilled development wells, with Ankleshwar Formation sandstones being the primary hydrocarbon-producing unit. Because the cores were not recovered, the log-based interpretation is used to characterize the YCS Formation, encountered in all of the wells.

Using the Cambay Basin-specific empirical relationship (equation 2), as established by Tyagi et al. (2011) from core data, the estimated Ro was found to be in the range of 0.8%–1%. A similar range of R_o was also reported by other workers. Figure 5 illustrates the compilation of the reported vitrinite reflectance values from various parts of the Cambay Basin, which indicates that our findings are well-correlated with the ones reported by Ariketi et al. (2017a), Singh et al. (2018), and Hafiz et al. (2020). These values imply that the YCS attained main to peak oil generation maturity. Based on the interpreted R_o%, an average value of 9.8 has been estimated against LOM in the studied YCS intervals from four wells. For the resistivity-sonic overlay method (Passey et al., 1990), both logs were scaled appropriately so that one resistivity log cycle corresponds to 60 μs/ft sonic intervals. In the studied wells, 2.5 ohm-m and 65 μs/ft were considered to be Rbase and Δtbase, which were used in equation 3. The organic content assessment from one of the wireline logs is presented in Figure 6. The ΔLog R method has estimated a range of 0.5–2.67 wt% TOC in the studied intervals, with an average value of 1.8 wt%. Estimated TOCs from the other three wells (W-11, W-13, and W-14) are presented in Figure 7. The density log-derived TOC estimates range between 0.5 and 3.5 wt%, which closely follows the trend of the ΔLog R-based TOC values (Figures 6 and 7); hence, it confirms the average TOC interpretation from Passey's method. Table 5 summarizes the estimated TOC values in the studied shale intervals. Ruble et al. (2012) provide a simple guideline for TOC limits (e.g., TOC < 0.5, poor; 0.5–1, fair; 1–2, good; 2–4, very good; and TOC > 4, excellent) to characterize the quality of organic richness for prospect evaluation. Following the same guideline for TOC characterization of YCS, the studied wells are considered comprise "*good-*" to "*very good*"-quality source rock. The estimated TOC values from all of the wells are combined, indicating an average TOC value of 2–2.5 wt%. We compiled all of the core-based TOC measurements as reported from multiple studies on the Cambay Shale Group to corroborate our interpretations, and our results are found to be well correlated in the measured range (Figure 8).

BI

To access a reliable model of brittleness and ductility of the targeted YCS in the absence of measured V_S, we used four well-known V_S models during the estimation of BI. Figure 9 represents the estimated V_S models together with the gamma-ray, lithology, and V_P log from one of the studied wells. Among all four models, the Han (1986) model and the Castagna et al. (1985) model-derived V_S estimates indicate the upper and lower bounds, respectively. Here, we realized various V_S estimates based on well-established and widely used models but we do not discuss which model is most suitable in practice due to the lack of availability of the measured V_S log. These estimates combined with the RPT analyses of the studied shales help to realize a

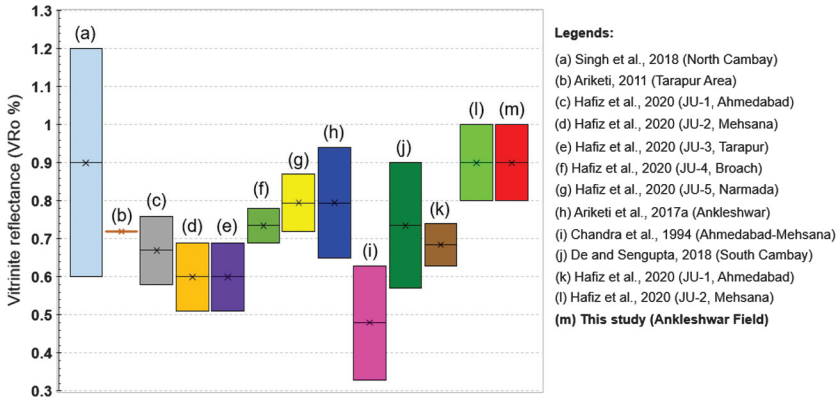

Figure 5. Represents the compilation of the published vitrinite reflectance (VR_o%) results from the Cambay Shales encountered in various parts of the studied basin.

DOI:10.1190/INT-2020-0133.1

range of V_P/V_S values that may exist in a real-case scenario. Figure 10 demonstrates the crossplot of P-impedance versus V_P/V_S ratio and lambda-rho versus mu-rho templates superimposed with log data from the studied shales. It can be seen from the templates that the YCS contains a wide range of clay content, mostly between 20% and 40%, with a nonlinear compaction trend (the deeper the formation is, the higher the P-impedance is). Moreover, the porosity of the studied samples has a range predominantly within 10%–22%, except some samples have values of less than 6%, which are consistent with those obtained from the well data and depth trend analysis. The constructed RPTs can be useful to quantify the well and the seismic data for precise estimation of the porosity, mineralogy, and BI, if available in the future for detailed study on shale prospects from this basin.

The mineralogy and elastic property-based BI values using the equations, as given by Tables 3 and 4, are illustrated in Figure 11. The BI interpretation guideline by Perez Altamar and Marfurt (2014) suggests that a BI value of <0.16 indicates highly ductile rocks, BI of 0.16–0.32 represents moderately to low ductile rocks, BI of 0.32–0.48 is indicative of less brittle rocks, and BI of >0.48 signifies highly brittle rocks. Mineralogical composition-based indices reveal that the studied shales of the Younger Cambay Group ranged between 0.2 and 0.72 and hence fall into a wide span of classification covering less-ductile to brittle regions with a majority being in the brittle zone. This is, however, not the exact case for BI calculation based on elastic properties, indicating mostly higher brittleness – less-brittle to highly brittle transition behavior, with a value ranging from 0.41 to 0.83. Similar output differences between lithology and elastic moduli-based approaches have also been reported by Nooraiepour et al. (2017b) on their study of the mechanical strength of cap rock mudstone from the Norwegian North Sea, although the mineralogy data frequency is much less and might not be sufficient enough to truly reflect the entire section. Nonetheless, some preliminary conclusions can be drawn duly supported by other related studies from the same region. To convey

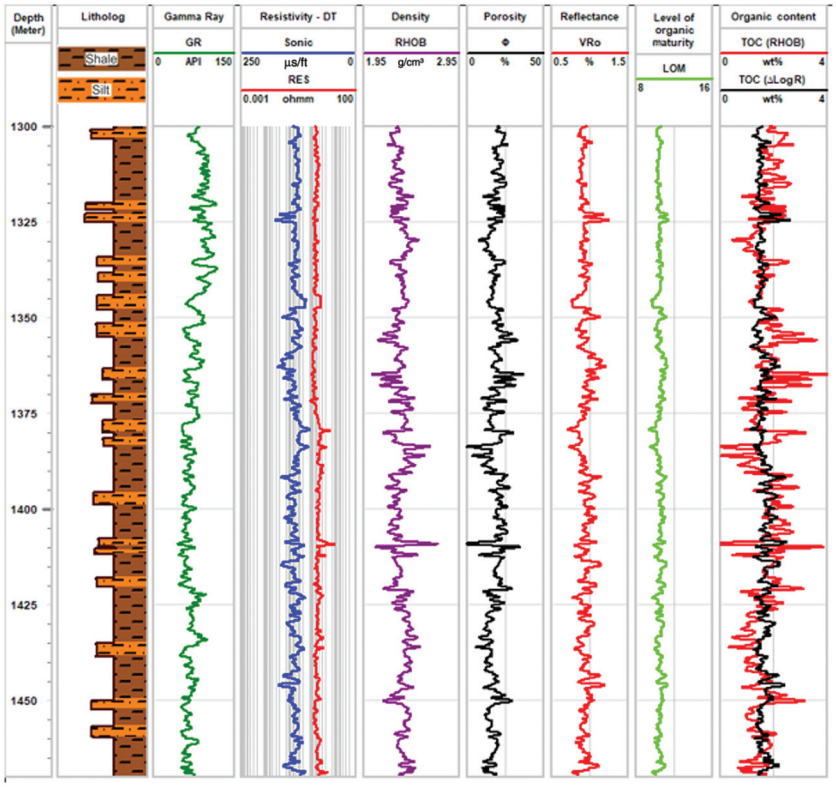

Figure 6. Represents the organic content assessment (R_o%, LOM, and TOC) from well W-12, together with the lithology, gamma-ray, resistivity-sonic overlay, density, and porosity logs. The TOC is estimated from the method as well as the density logs.

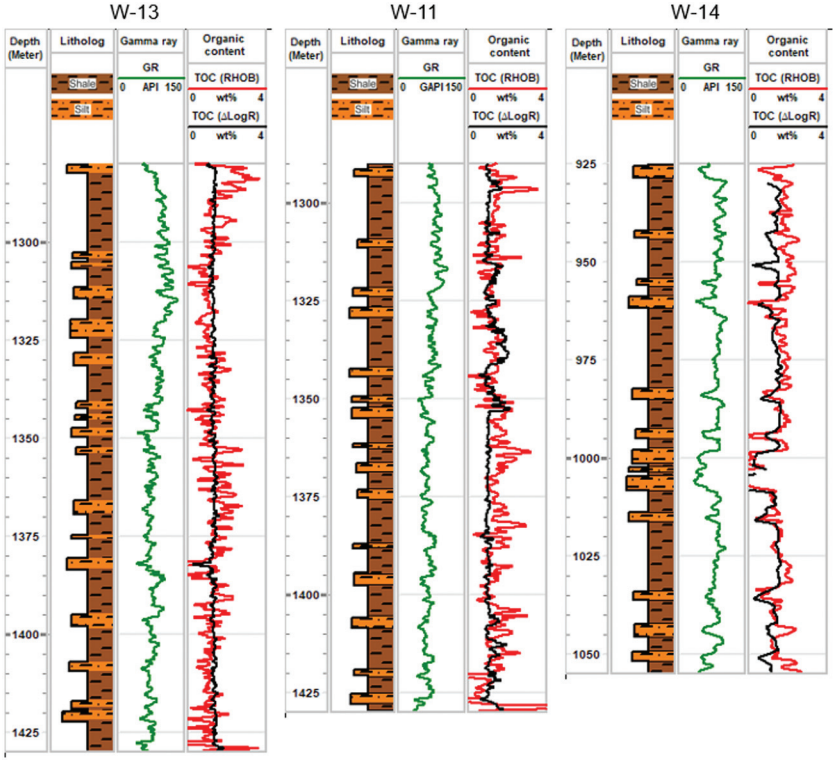

Figure 7. Estimated TOC together with the lithology and gamma-ray log from wells W-11, W-13, and W-14, respectively. The TOC is estimated from the method as well as the density logs.

DOI:10.1190/INT-2020-0133.1

a basis for discussion, various published models with a variety of mineral assemblages were used for the quantification of brittleness and ductility. As depicted in Figure 11c, out of four well-known models, the models proposed by Jarvie et al. (2007) and Wang and Gale (2009) provide the lower bounds and Glorioso and Rattia (2012) and Jin et al. (2014) suggest the upper bounds of composition-based brittleness. In the case of elastic property-based indices, a narrow range in the variation of BI is observed, although four different widely used V_S models are considered (Figure 11d and 11e). Moreover, Grieser and Bray (2007) and Rickman et al. (2008) suggest the lower and upper bounds of brittleness, respectively. The model proposed by Guo et al. (2012) (M3, see Figure 11f) also correlates well and demonstrates a similar trend as shown by others (M1 and M2). Moreover, it is important to note that the studied shale samples, as a whole, mainly retain the brittleness behavior, indicating a good ability to endure significant strain and a lower likelihood of fracture. This seems justified because as reported by Nobakht et al. (2013) highly brittle rocks are more responsive to hydraulic fracturing and hence favorable.

Table 5. TOC estimated by the delta LogR method studied shale intervals of the Cambay Basin in western India.

Well no.	Intervals (m)	TOC range (wt%)
W-11	1280–1425	1.00–2.48
W-12	1295–1475	1.31–2.67
W-13	1280–1425	1.02–1.61
W-14	930–1060	0.50–1.73

A compilation and comparison of the Cambay Shale brittleness values reported by various researchers is presented in Figure 12. Our findings are in a qualitative good agreement with earlier findings by Ariketi et al. (2017b) for the equivalent Cambay Shale interval in the offset Ankleshwar area, where the BI range is interpreted to be within 0.44 to 0.7 based on the elastic moduli and X-ray diffraction analyses. Kumar et al. (2018) report a brittleness range of 0.22–0.55 (low to medium brittleness), based on the mineralogical composition analysis using drill cutting samples (seven samples within the interval of 1735–1990 m) of the OCS from Ahmedabad block, north Cambay Basin. In a recent study, Hafiz et al. (2020) report a very wide range of BI from this basin, that is, 0.08–0.57, as obtained from mineralogical models. This implies that the brittleness characteristics of the Cambay Shale are not uniform throughout the basin and that south Cambay Shales are comparatively more brittle than those of the northern part of the basin. This could be attributed to clay content; north Cambay Shales are more clay-rich than the southern ones. Further, Sharma and Sircar (2018) report an average BI of 0.20 from the Cambay Shale samples (the exact location is not provided) using

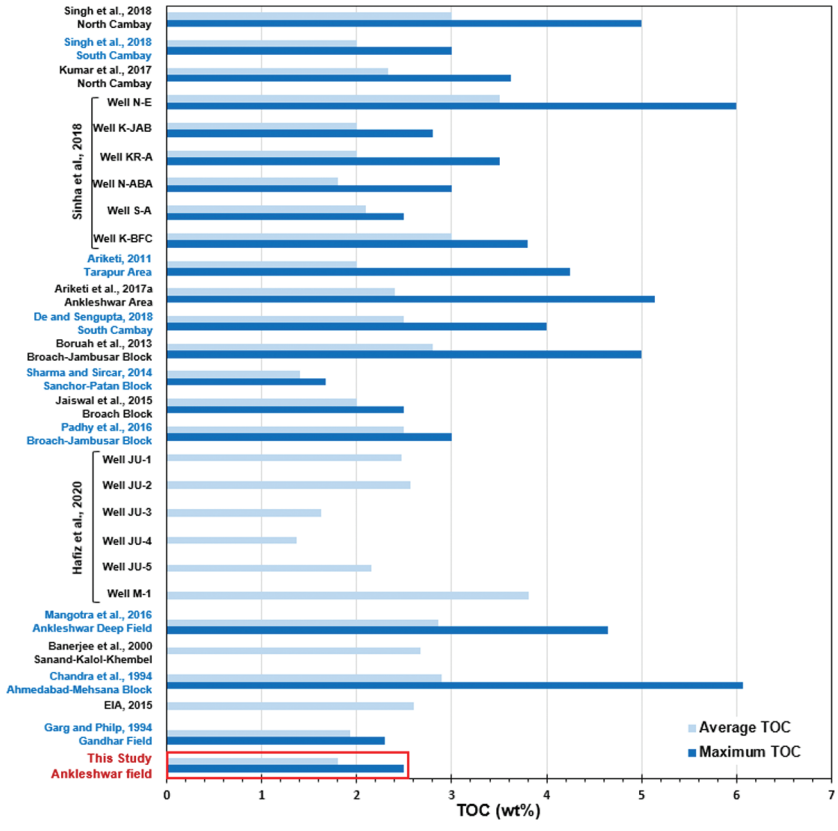

Figure 8. Compilation of all core-based direct TOC measurements (average and maximum values) from the Cambay Shales encountered in various parts of the Cambay Basin. The results from this study have been plotted on the same scale for comparison (marked by a red square).

DOI:10.1190/INT-2020-0133.1

mineralogy-based analysis but could not conclude on the shale brittleness due to the limited data set.

As can be seen from Figure 11e and 11f, it is important to note a local increase in brittleness against two depth intervals (i.e., 1346 and 1385 m), which may be speculated due to increased silica content (i.e., a decreased shale volume fraction). A comprehensive study is a prerequisite to substantiate this conjecture, although a notable correlation between the gamma-ray data and brittleness indices has been identified. To understand the effect of the lithology/shale volume (Vshale in fraction) on the brittle or ductile behavior of rocks, a crossplot between BI and Vshale was prepared and is displayed in Figure 13. Rocks with a relatively higher shale volume or clay content are more ductile. This suggests that the Eocene shales at a deeper burial depth (older) comprise less clay content with more TOC values; hence, they are more brittle when compared to the shallow shales (younger) with relatively lower TOC values. This has also been evidenced from the lambda-rho versus mu-rho template, where it can be clearly seen that mu-rho decreases as the clay content increases with a range of porosity values; however, Lambda-rho is characterized with an opposite trend (Figure 10b). A linear trend or relationship between BI and Vshale with a maximum correlation coefficient of 92.4 is observed, which is given below:

$$\mathrm{BI} = -1.032\,\mathrm{Vshale} + 1.295. \quad (19)$$

This trend line can be relatively convenient to model the BI from the shale volume when log-derived brittleness values are absent or scarce.

The PP and principal stress magnitudes

Methods for estimating the PP and in situ stress components have been discussed earlier in the "Analytical methods" section. The studied wells had three casing policies. The top section was drilled with a 26" bit, and a 20" casing was placed at approximately 175 m TVD. The second section, being drilled with a 12 ¼" bit and a 9 5/8" casing, was placed at 800 m TVD. The final section comprising Ankleshwar sandstones and YCS was drilled with a 8 ½" bit till target depth and completed with a 7" liner. To establish and understand the porosity compaction trend, a porosity depth trend (depth versus porosity plot) is portrayed in Figure 14a. Clearly, the retention of relatively higher porosities is noticed, starting at a depth of approximately

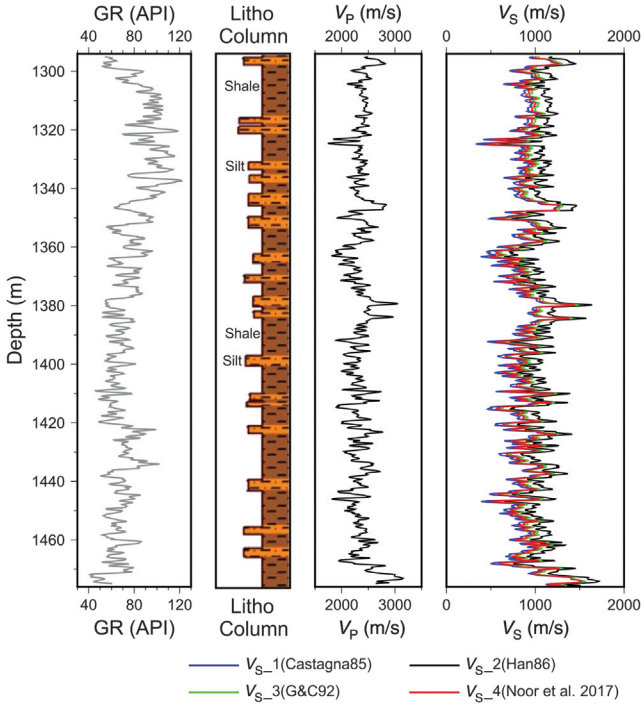

Figure 9. Estimated V_S logs together with the gamma-ray log and measured V_P log from one of the studied wells, W-12. The legend represents four well-known models for V_S prediction, for example, Castagna et al. (1985), Han (1986), Greenberg and Castagna (1992), and Nooraiepour et al. (2017a), respectively.

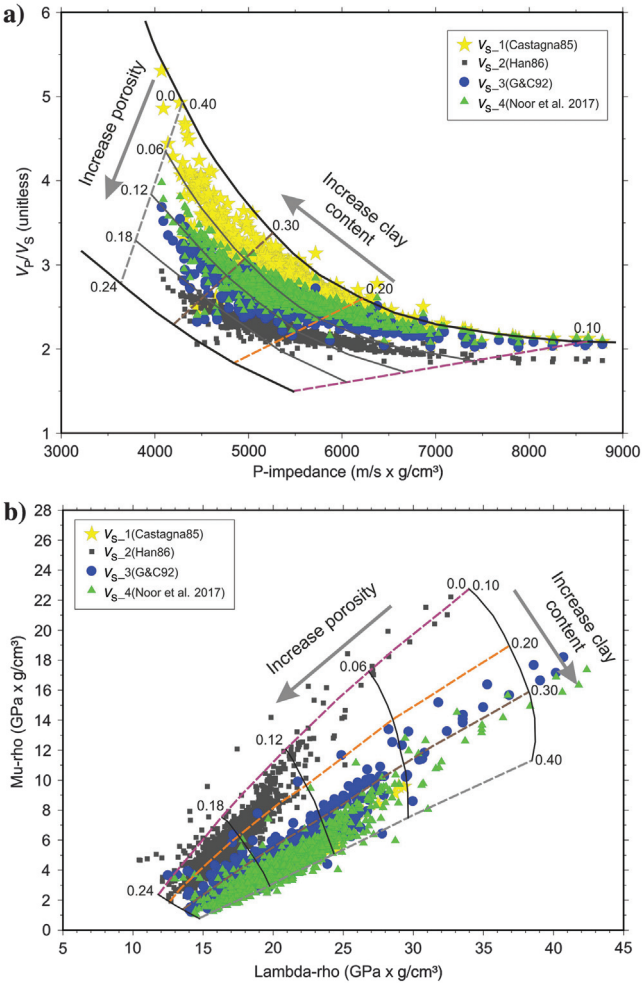

Figure 10. RPTs of (a) P-impedance versus V_P/V_S ratio (top) and (b) lambda-rho versus mu-rho (bottom) superimposed with log data comprising the Eocene Cambay Shales properties.

550 m TVD, which also marks the onset of the shale overpressure. This observation was translated to establish the NCT on the resistivity and compressional sonic slowness logs and was used for calculating PP using Eaton's method. A crossplot between the shale density and the compressional sonic slowness values provided a linear relationship in the Cambay Shale (Figure 14b), which implies the compaction disequilibrium to be the dominant mechanism behind the Cambay Shale overpressure. Any evidence of chemical compaction could not be found from the results. PP is calculated only against shales and is measured against sandstones. Downhole formation pressure measurements (MDT) were available from the Ankleshwar sandstone, which were the primary targets for these wells. Because MDT data were unavailable against the shale intervals, drilling mud weight indicated sufficient drilling mud overbalance and indirectly helped in PP estimation. Connection gases, influx/kick, pressure cavings, anomalous torque, and drag readings have not been reported from daily drilling reports available from the studied wells. These were incorporated in the analyses to calibrate the calculated PP. A maximum of 10.2 pounds per gallon equivalent (ppgE) PP gradient was estimated against the Cambay Shale, which was successfully drilled using a mud weight of 12.0–12.5 ppgE in the four wells. The calculated fracture pressure/gradient was also calibrated with LOT values, as available from the wells. The bottom-hole pressure has to be kept below the fracture pressure during horizontal drilling but above the fracture pressure while hydraulic fracturing to circumvent accidents, mud loss, and economic loss. FCps available from the LOT graphs have been used to estimate and calibrate the SH_{Max} magnitude. To understand the possible fracture initiation, propagation and reopening during shale resource exploitation in the studied field, a broad range of dynamic geomechanical parameters was estimated using the geophysical logs (Table 6) and calibrated with core-based results.

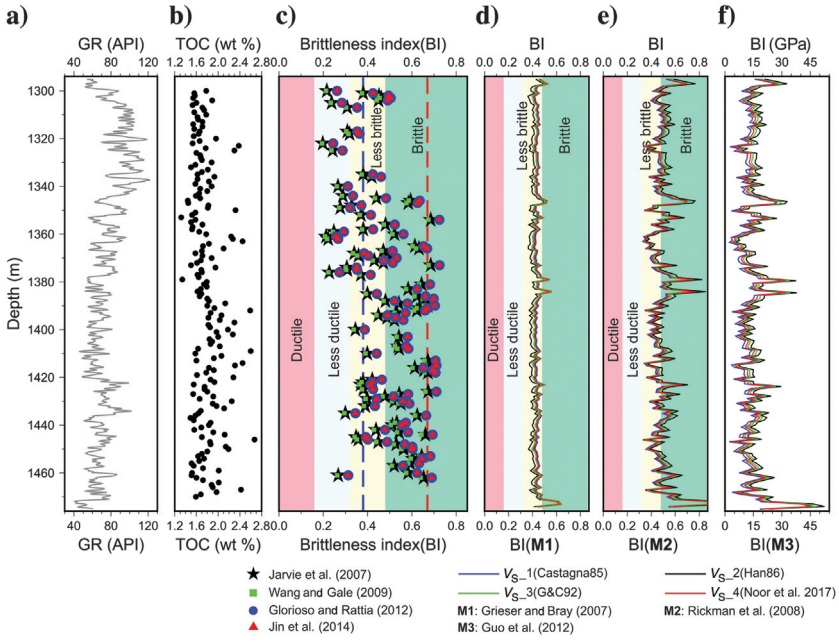

Figure 11. Evaluation of brittleness and ductility of the studied Eocene Cambay Shale horizons in well W-12. Representation of (a) measured gamma-ray log; (b) TOC values; (c) estimated brittleness indices based on mineralogical composition, estimated brittleness indices based on elastic properties: (d) model M1 (Grieser and Bray, 2007), (e) model M2 (Rickman et al., 2008), and (f) model M3 (Guo et al., 2012). The average brittleness behavior based on mineralogical composition, reported by earlier workers such as Ariketi et al. (2017a) from this study area (south Cambay), and Sharma and Sircar (2019) from the north Cambay basin are represented by the red dashed and blue dashed lines, respectively.

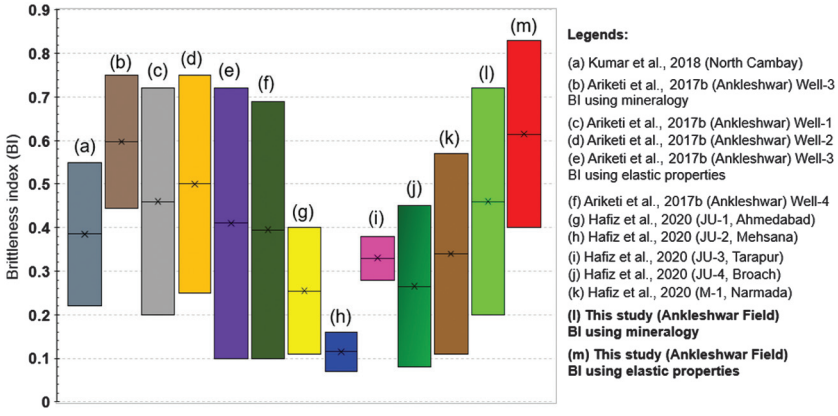

Figure 12. Compilation of the estimated BI, as obtained from the present study together with the reported BI ranges of the Cambay Shales encountered in various parts of the Cambay Basin.

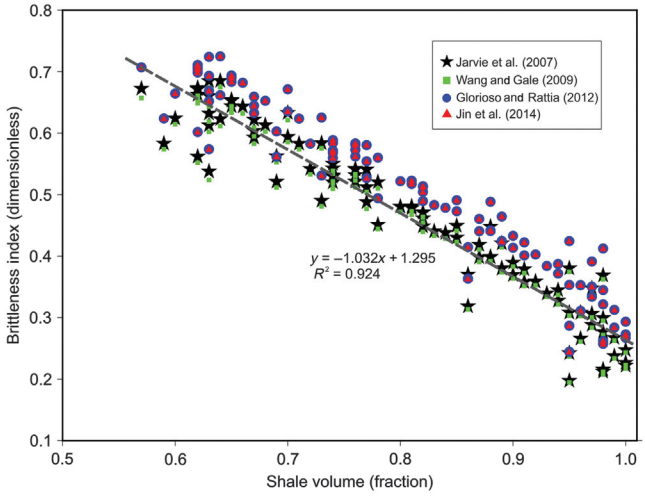

Figure 13. Crossplot of mineralogy-derived BI versus shale volume (Vshale) against the YCS intervals from one of the studied wells, well W-12. Vshale is computed from the gamma-ray log (please refer to Table 3).

The PP and stress measurements of one of the studied wells, well W-12, are given in Figure 15. The study reveals that the average overburden pressure (S_v) gradient is 21.2 MPa/km. The PP has been interpreted as slightly more than the hydrostatic pressure against the studied shale interval, with an average gradient of 10.5–11.5 MPa/km. The S_{hmin} and S_{HMax} are found to be 18.5 and 19.7 MPa/km; S_{eh} has an average 8.5–8.8 MPa/km gradient, but an S_{ev} gradient is comparatively more with an average of 9.5–9.9 MPa/km against the studied YCS intervals. The relative magnitudes of the three stress tensors show that S_v is the highest (S_1) and S_{hmin} is the lowest (S_3) ($S_{hmin} < S_{HMax} < S_v$). As per Anderson's classification, our study area has been established as a normal fault tectonic regime. Furthermore, to understand the relationships of various dynamic geomechanical parameters with TOC (wt%), multiple crossplots were established and are illustrated in Figure 16. The dynamic Young's modulus, shear modulus, and bulk modulus vary inversely with the TOC, whereas the Poisson's ratio has a positive relationship with the organic content.

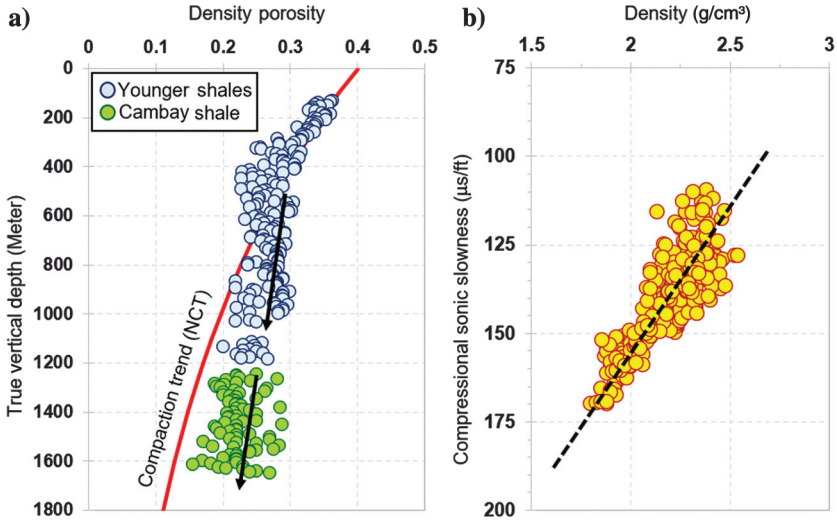

Figure 14. (a) The depth versus porosity trend is presented as a compaction trend line, indicating the onset of deviation at approximately 550 m TVD. Cambay Shales are also found to retain more porosities beyond the compaction line generating overpressure. (b) A crossplot between the density and the compressional sonic slowness provides a linear relationship, indicating the compaction disequilibrium as one of the dominating factors behind the overpressure in the studied shales.

Table 6. Estimated dynamic geomechanical properties with their mean values across the YCS from the four studied wells (V_P/V_S, ratio of P-wave velocity to S-wave velocity; S0, cohesive strength; u, friction coefficient; ν, Poisson's ratio; E, Young's modulus; G, shear modulus; and K, bulk modulus).

Well no.	Intervals (m)	V_P/V_S	S0 (MPa)	u	ν	E (GPa)	G (GPa)	K (GPa)
W-11	1280–1425	1.6–2.6	2.9–6.1	0.3–0.5	0.3–0.4	4.3–9.2	1.3–4.5	5.8–9.5
W-12	1295–1475	1.6–2.5	2.8–6.0	0.2–0.5	0.2–0.4	3.6–9.2	1.4–4.4	4.1–9.4
W-13	1280–1425	1.4–1.9	4.2–5.8	0.4–0.6	0.2–0.4	5.1–9.9	2.6–4.8	4.9–10.0
W-14	930–1060	1.2–2.3	3.0–6.4	0.3–0.6	0.2–0.3	2.8–10.0	1.6–3.8	4.5–9.2
Mean values =		1.80	4.50	0.50	0.31	6.80	2.50	6.40

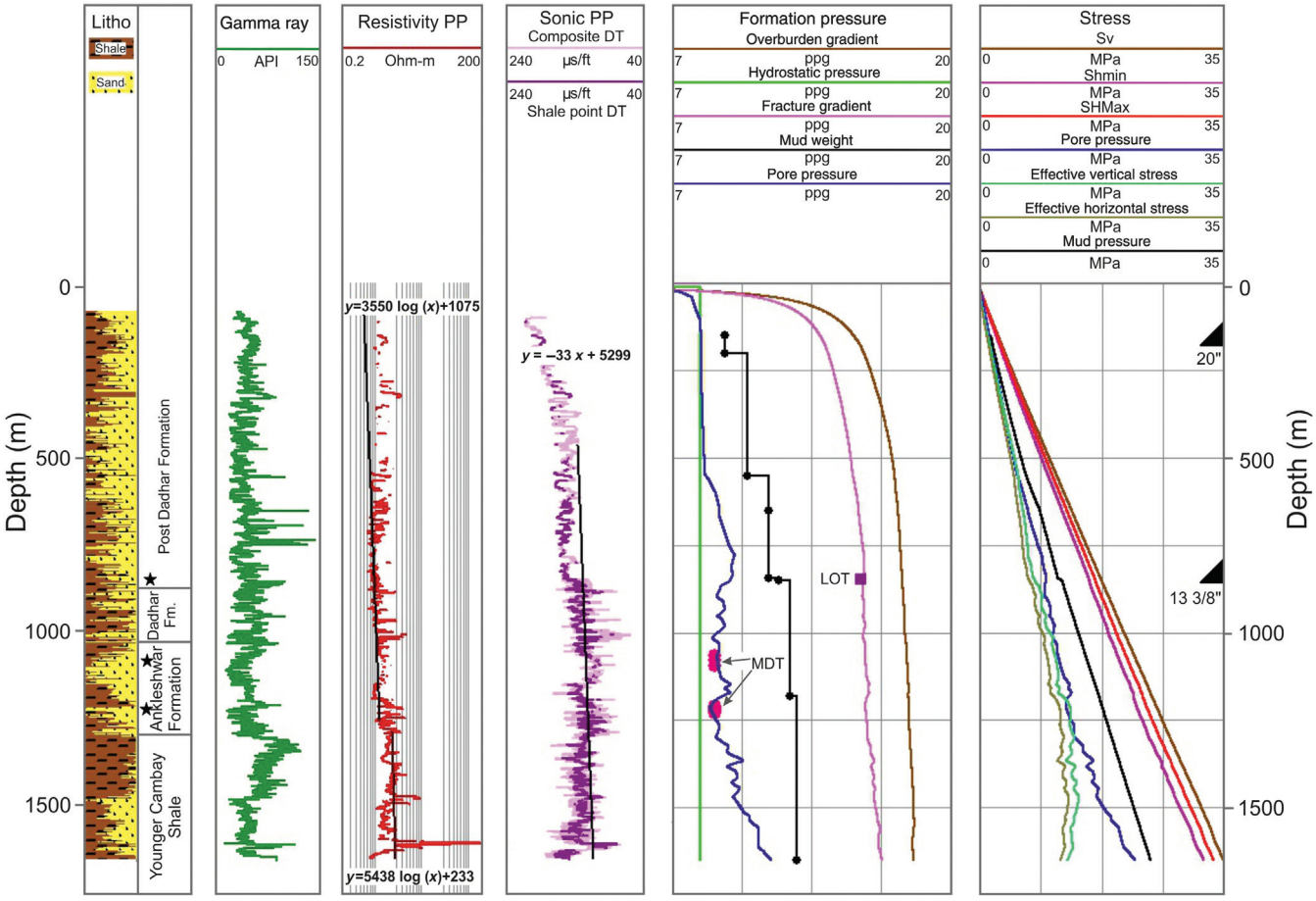

Figure 15. Representation of a geomechanical model of the well W-12 from the Ankleshwar field, displaying various formation pressure gradients (e.g., overburden, fracture, PP, etc.) and stress magnitudes along with the NCTs on resistivity and sonic logs, mud weight, downhole pressure measurements (MDT and LOT), and casing points. The black stars represent the location of downhole direct pressure measurements.

Figure 16. Crossplots of various estimated dynamic geomechanical modulus versus TOC (wt%), representing the YCS intervals. The legend represents the wells used in this study.

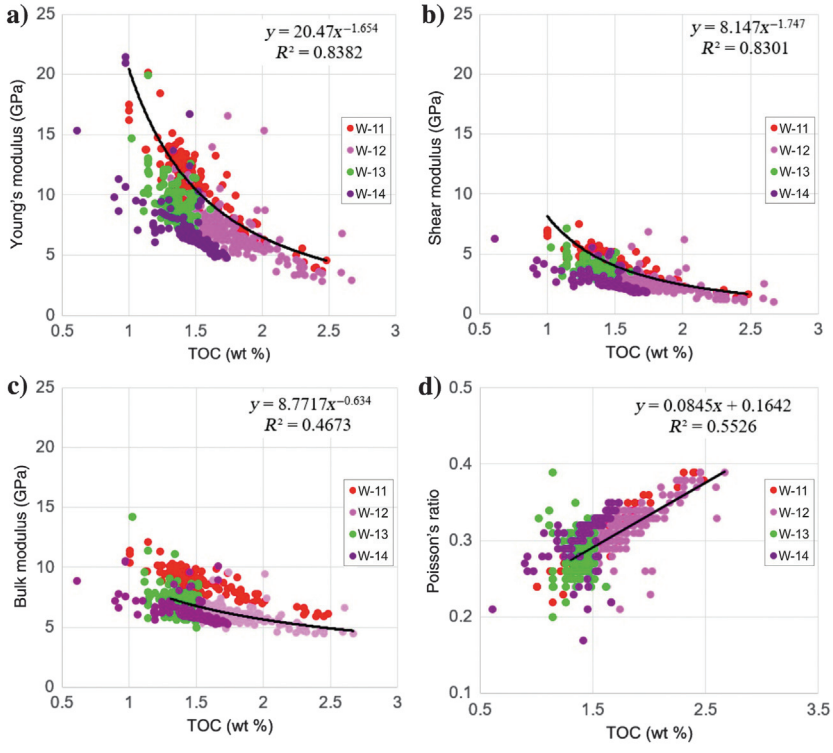

Conclusion

We have evaluated the YCS interval of the Cambay Basin in terms of its R_o and organic content, and we characterized its intrinsic geomechanical properties that have direct implications in a successful drilling and completion strategy. On the four studied wells, the YCS interval has an average R_o% of 0.8–1.0 and the TOC of 1.8 wt% was interpreted from the studied wells, which is indicative of thermally well-matured shales with good to very good organic content. The organic matter within the studied YCS intervals originated in a terrestrial or marine environment, which was deposited during the end of a transgressive phase with a sufficient amount of oxygen supply. The mineralogy-based and elastic property-based estimated BI suggest that the YCS group is mostly in a brittle zone. In other words, the YCS interval can withstand a significant amount of strain before fracture and is a potential candidate for hydrofracturing. Further, in the YCS interval, an increase in the shale volume decreases the BI values, whereas an increase in the TOC decreases the Young's, bulk, and shear moduli but increases the Poisson's ratio. Analyses of the stress tensors indicate mainly a normal fault tectonic regime, with a mostly hydrostatic pressure regime till the top of the Cambay Shale, whereas a little more than the hydrostatic pressure has been interpreted against the targeted shales. However, drilling these zones with >11 ppgE mud weight was proven to be devoid of complications and, hence, was suggested for shale-gas exploration in the studied region. Moreover, it is essential to realize that core-based results and advanced geophysical logs are vital for a detailed characterization of an unconventional resource play. The integrated workflow presented here provides a good, cost-effective alternative to characterize a shale interval within a producing conventional hydrocarbon field for unconventional resource purposes, especially when core data are unavailable.

Acknowledgments

We sincerely appreciate the editor and the anonymous reviewers for providing fruitful suggestions that significantly improved the quality of the work. The authors gratefully thank Oil and Natural Gas Corporation Limited for providing the data set. This study was supported by a DST Inspire Faculty research grant (grant no. DST/INSPIRE/04/2016/000174) for which SSG is obliged to DST, government of India. SSG is grateful to the Director of CSIR-NGRI for all the support and for giving consent to publish the results. SS expresses his sincere gratitude to Geologix Limited for providing access to the unconventional log analysis module of the GEO suite of software for part of the data analyses. SV would like to thank AASPI consortium sponsors for financial support.

Data and materials availability

Data associated with this research are confidential and cannot be released.

References

Ariketi, R., 2011, Estimation of level of organic maturity (LOM) and total organic carbon (TOC) in absence of geochemical data by using resistivity and density logs — Example from Cambay Shale, Tarapur area, Cambay Basin, India: Journal of Indian Association of Sedimentologists, **30**, 55–63.

Ariketi, R., U. K. Bhui, S. Chandra, and S. Biswal, 2017a, Evaluation of organic richness and thermal maturity of Cambay Shale Formation for shale gas exploration — A study from Ankleshwar area, Cambay Basin, India: Geohorizons, **22**, 17–27.

Ariketi, R., U. K. Bhui, S. Chandra, and S. Biswal, 2017b, Brittleness modeling of Cambay shale formation for shale gas exploration: A study from Ankleshwar area, Cambay Basin, India: Journal of Petroleum Exploration and Production Technology, **7**, 911–923, doi: 10.1007/s13202-017-0326-2.

Bakshi, T., B. K. Prusty, K. Pathak, and S. K. Pal, 2017, Pore characteristics of Damodar valley shale and their effect on gas storage potential: Journal of Petroleum Science and Engineering, **162**, 725–735, doi: 10.1016/j.petrol.2017.10.091.

Banerjee, A., M. Jha, A. K. Mittal, N. J. Thomas, and K. N. Misra, 2000, The effective source rocks in the North Cambay Basin, India: Marine and Petroleum Geology, **17**, 1111–1129, doi: 10.1016/S0264-8172(00)00049-0.

Biswas, S. K., R. Ariketi, R. Dubey, and S. Chandra, 2013, Shale gas evaluation of Cambay Shale Formation in Tarapur Syncline, Cambay Basin, India — A seismo-geological approach: 10th Biennial International Conference and Exposition, 142.

Boruah, A., M. A. Rasheed, S. Z. Hasan, P. H. Rao, and B. Kumar, 2013, Application of geochemistry in shale gas exploration: A case study from Cambay Basin, Gujarat, India: Goldschmidt-23rd Conference.

Busch, A., and A. Amann-Hildenbrand, 2013, Predicting capilarity of mudrocks: Marine and Petroleum Geology, **45**, 208–223, doi: 10.1016/j.marpetgeo.2013.05.005.

Carcione, J. M., 2000, A model for seismic velocity and attenuation in petroleum source rocks an acoustic model for petroleum source rocks: Geophysics, **65**, 1080–1092, doi: 10.1190/1.1444801.

Castagna, J. P., M. L. Batzle, and R. L. Eastwood, 1985, Relationships between compressional-wave and shear-wave velocities in clastic silicate rocks: Geophysics, **50**, 571–581, doi: 10.1190/1.1441933.

Chandra, K., C. S. Mishra, U. Samanta, A. Gupta, and K. L. Mehrotra, 1994, Correlation of different maturity parameters in the Ahmedabad-Mehsana block of the Cambay basin: Organic Geochemistry, **21**, 313–321, doi: 10.1016/0146-6380(94)90193-7.

Dang, S. T., C. H. Sondergeld, and C. S. Rai, 2016, A new approach to measuring organic density: Petrophysics, **57**, 112–120.

De, S., and D. Sengupta, 2018, Evaluation of total organic carbon content, thermal maturity, clay-mineralogy and depositional environment of Cambay Shale Formation, Cambay Basin, India: Geophysical Research Abstracts, 20, EGU 2018-3801.

Eaton, B. A., 1975, The equation for geopressure prediction from well logs: 50th Annual Fall Meeting of the Society of Petroleum Engineers of AIME, SPE 5544, 11.

EIA, 2015, Technically recoverable shale oil and shale gas resources: India and Pakistan. Independent Statistics and Analysis, U.S. Department of Energy, Washington, DC 20585.

Ganguli, S. S., 2017, Integrated reservoir studies for CO_2-enhanced oil recovery and sequestration: Application to an Indian mature oil field, 1st ed.: Springer International Publishing.

Ganguli, S. S., P. Kumar, and V. P. Dimri, 2019, Seismic anisotropy of a fractured rock during CO_2 injection: A feasibility study: Acta Geophysica, **67**, 141–148, doi: 10.1007/s11600-019-00246-w.

Ganguli, S. S., and S. Sen, 2020, Investigation of present-day in-situ stresses and pore pressure in the south Cambay Basin, western India: Implications for drilling, reservoir development and fault reactivation: Marine and Petroleum Geology, **118**, 104422, doi: 10.1016/j.marpetgeo.2020.104422.

Ganguli, S. S., N. Vedanti, I. Akervoll, P. E. Bergmo, R. P. Srivastava, and V. P. Dimri, 2017, Investigating CO2-enhanced oil recovery potential for a mature oil field: A case study based on Ankleshwar oil field, Cambay Basin, India: Arabian Journal of Geosciences, **10**, 124, doi: 10.1007/s12517-017-2940-1.

Ganguli, S. S., N. Vedanti, I. Akervoll, and V. P. Dimri, 2016a, Assessing the feasibility of CO_2-enhanced oil recovery and storage in mature oil field: A case study from Cambay basin: Journal of the Geological Society of India, **88**, 273–280, doi: 10.1007/s12594-016-0490-x.

Ganguli, S. S., N. Vedanti, and V. P. Dimri, 2016b, 4D reservoir characterization using well log data for feasible CO_2-enhanced oil recovery at Ankleshwar, Cambay Basin — A rock physics diagnostic and modeling approach: Journal of Applied Geophysics, **135**, 111–121, doi: 10.1016/j.jappgeo.2016.10.007.

Ganguli, S. S., N. Vedanti, O. P. Pandey, and V. P. Dimri, 2018, Deep thermal regime, temperature induced over-pressured zone and implications for hydrocarbon potential in the Ankleshwar oil field, Cambay basin, India: Journal of Asian Earth Sciences, **161**, 93–102, doi: 10.1016/j.jseaes.2018.05.005.

Garg, A. K., and R. P. Philp, 1994, Pyrolysis-gas chromatography of asphaltenes/kerogens from source rocks of the Gandhar Field, Cambay Basin, India: Organic Geochemistry, **21**, 383–392, doi: 10.1016/0146-6380(94)90200-3.

Ghazwani, A., R. Littke, G. Gaus, and C. Hartkopf-Fröder, 2018, Assessment of unconventional shale gas potential of organic-rich Mississippian and Lower Pennsylvanian sediments in western Germany: International Journal of Coal Geology, **198**, 29–47, doi: 10.1016/j.coal.2018.08.008.

Glaser, K. S., C. K. Miller, G. M. Johnson, R. L. Kleinberg, and W. D. Pennington, 2014, Seeking the sweet spot: Reservoir and completion quality in organic shales: Oilfield Review, **25**, 16–29.

Glorioso, J. C., and A. J. Rattia, 2012, Unconventional reservoirs: Basic petrophysical concepts for shale gas: Society of Petroleum Engineers.

Greenberg, M. L., and J. P. Castagna, 1992, Shear-wave velocity estimation in porous rocks: Theoretical formulation, preliminary verification and applications: Geophysical Prospecting, **40**, 195–209, doi: 10.1111/j.1365-2478.1992.tb00371.x.

Grieser, W. V., and J. M. Bray, 2007, Identification of production potential in unconventional reservoirs: Production and Operations Symposium.

Guo, Z., M. Chapman, and X. Li, 2012, A shale rock physics model and its application in the prediction of brittleness index, mineralogy, and porosity of the Barnett Shale: 82nd Annual International Meeting, SEG, Expanded Abstracts, doi: 10.1190/segam2012-0777.1.

Hafiz, M., N. Hakhoo, G. M. Bhat, S. Kanungo, B. Thusu, J. Craig, and W. Ahmed, 2020, Source potential and reservoir characterization of the Cambay Shale, Cambay Basin, India: Implications for tight gas and tight oil resource development: AAPG Bulletin, **104**, 1707–1749, doi: 10.1306/03162017174.

Han, D. H., 1986, Effects of porosity and clay content on acoustic properties of sandstones and unconsolidated sediments: Ph.D. thesis, Stanford University, Department of Geophysics, Stanford, USA.

Hansen, J. A., N. H. Mondol, and M. Fawad, 2019, Organic content and maturation effects on elastic properties of source rock shales in the Central North Sea: Interpretation, **7**, no. 2, T477–T497, doi: 10.1190/INT-2018-0105.1.

Jaiswal, R. K., S. K. Shrivastava, and U. S. D. Pandey, 2015, Identification of shale gas by VSP & well log data: 11th Biennial International Conference and Exposition by SPG.

Jaiswal, S., and B. Bhattacharya, 2018, Characterization of middle Eocene tide-influenced delta: A study from core samples of Hazad Member, Ankleshwar Formation, South Cambay Basin, India: Journal of Earth System Science, **127**, 65, doi: 10.1007/s12040-018-0966-8.

Jarvie, D. M., B. L. Claxton, F. Henk, and J. T. Breyer, 2001, Oil and shale gas from the Barnett Shale, Ft. Worth Basin, Texas: AAPG National Convention, AAPG Bull., 85, No. 13 (Supplement), A100.

Jarvie, D. M., R. J. Hill, T. E. Ruble, and R. M. Pollastro, 2007, Unconventional shale-gas systems: The Mississippian Barnett Shale of north-central Texas as one model for thermogenic shale-gas assessment: AAPG Bulletin, **91**, 475–499, doi: 10.1306/12190606068.

Jin, X., S. N. Shah, J. -C. Roegiers, and B. Zhang, 2014, Fracability evaluation in shale reservoirs — An integrated petrophysics and geomechanics approach: Society of Petroleum Engineers.

Kenomore, M., M. Hassan, H. Dhakal, and A. Shah, 2017, Total organic carbon evaluation of the Bowland Shale Formation in the Upper Bowland of the Widmerpool Gulf: Journal of Petroleum Science and Engineering, **150**, 137–145, doi: 10.1016/j.petrol.2016.11.040.

Kumar, S., S. Das, R. Bastia, and K. Ojha, 2018, Mineralogical and morphological characterization of Older Cambay Shale from North Cambay Basin, India: Implication for shale oil/gas development: Marine and Petroleum Geology, **97**, 339–354, doi: 10.1016/j.marpetgeo.2018.07.020.

Kumar, S., K. Ojha, R. Bastia, K. Garg, S. Das, and D. Mohanty, 2017, Evaluation of Eocene source rock for potential shale oil and gas generation in north Cambay Basin, India: Marine and Petroleum Geology, **88**, 141–154, doi: 10.1016/j.marpetgeo.2017.08.015.

Liu, Y., X. Tang, J. Zhang, X. Mo, H. Huang, and Z. Liu, 2018, Geochemical characteristics of the extremely high thermal maturity transitional shale gas in the Southern North China Basin (SNCB) and its differences with marine shale gas: International Journal of Coal Geology, **194**, 33–44, doi: 10.1016/j.coal.2018.05.005.

Mallick, R. K., and S. V. Raju, 1995, Thermal maturity evaluation by sonic log and seismic velocity analysis in parts of Upper Assam Basin, India: Organic Geochemistry, **23**, 871–879, doi: 10.1016/0146-6380(95)00088-7.

Matthews, W. R., and J. Kelly, 1967, How to predict formation pressure and fracture gradient: Oil and Gas, **65**, 92–106.

Mishra, S., D. Mani, S. Kavitha, M. S. Kalpana, D. J. Patil, D. U. Vyas, and A. M. Dayal, 2014, Organic matter characteristics and gas generation potential of the Tertiary shales from NW Kutch, India: Journal of Petroleum science and Engineering, **124**, 114–121, doi: 10.1016/j.petrol.2014.10.019.

Mukherjee, M. K., 1981, Evolution of Anklesvar Anticline, Cambay Basin, India: AAPG Bulletin, **65**, 336–343, doi: 10.1306/2F9197D3-16CE-11D7-8645000102C1865D.

Mullen, M. J., R. Roundtree, and G. A. Turk, 2007, A composite determination of mechanical rock properties for stimulation design (what to do when you don't have a sonic log): Gas Technology Symposium, Paper SPE-109139-MS.

Nobakht, M., C. R. Clarkson, and D. Kaviani, 2013, New type curves for analyzing horizontal well with multiple fractures in shale gas reservoirs: Journal of Natural Gas Science and Engineering, **10**, 99–112, doi: 10.1016/j.jngse.2012.09.002.

Nooraiepour, M., B. G. Haile, and H. Hellevang, 2017b, Compaction and mechanical strength of Middle Miocene mudstones in the Norwegian North Sea — The major seal for the Skade CO_2 storage reservoir: International Journal of Greenhouse Gas Control, **67**, 49–59, doi: 10.1016/j.ijggc.2017.10.016.

Nooraiepour, M., N. H. Mondol, H. Hellevang, and K. Bjørlykke, 2017a, Experimental mechanical compaction of reconstituted shale and mudstone aggregates: Investigation of petrophysical and acoustic properties of SW Barents Sea cap rock sequences: Marine and Petroleum Geology, **80**, 265–292, doi: 10.1016/j.marpetgeo.2016.12.003.

Padhy, P. K., A. Kumar, Y. R. Chandra, S. K. Das, S. K. Jha, and D. R. Advani, 2016, Shale oil exploration from paleocene-early eocene sequence in Cambay Rift Basin, India: Proceedings of the Indian National Science Academy, **82**, 945–963, doi: 10.16943/ptinsa/2016/48495.

Passey, Q. R., S. Creaney, J. B. Kulla, F. J. Moretti, and J. D. Stroud, 1990, Practical model for organic richness from porosity and resistivity logs: AAPG Bulletin, **74**, 1777–1794, doi: 10.1306/0C9B25C9-1710-11D7-8645000102C1865D.

Perez Altamar, R., and K. Marfurt, 2014, Mineralogy-based brittleness prediction from surface seismic data: Application to the Barnett Shale: Interpretation, **2**, no. 4, T255–T271, doi: 10.1190/INT-2013-0161.1.

Plumb, R. A., K. F. Evans, and T. Engelder, 1991, Geophysical log responses and their correlation with bed-to-bed stress contrasts in Paleozoic rocks, Appalachian Plateau, New York: Journal of Geophysical Research, Solid Earth, **96**, 14509–14528, doi: 10.1029/91JB00896.

Radwan, A. E., and S. Sen, 2020, Stress path analysis for characterization of in situ stress state and effect of reservoir depletion on present-day stress magnitudes: Reservoir geomechanical modeling in the Gulf of Suez Rift Basin, Egypt: Natural Resources Research.

Rahman, M. J., M. Fawad, and N. H. Mondol, 2020, Organic-rich shale caprock properties of potential CO2 storage sites in the northern North Sea, offshore Norway: Marine and Petroleum Geology, **122**, 104665, doi: 10.1016/j.marpetgeo.2020.104665.

Rajabi, M., M. Tingay, and O. Heidbach, 2016, The present-day state of tectonic stress in the Darling Basin, Australia: Implications for exploration and production: Marine and Petroleum Geology, **77**, 776–790, doi: 10.1016/j.marpetgeo.2016.07.021.

Rasmussen, B., 2005, Evidence for pervasive petroleum generation and migration in 3.2 and 2.63 Ga shales: Geology, **33**, 497, doi: 10.1130/G21316.1.

Rickman, R., M. J. Mullen, J. E. Petre, W. V. Grieser, and D. Kundert, 2008, A practical use of shale petrophysics for stimulation design optimization: All shale plays are not clones of the Barnett Shale: Annual Technical Conference and Exhibition, SPE, Extended Abstracts, SPE-115258-MS.

Ruble, T. E., R. J. Drozd, and W. A. Heck, 2012, Practical geochemical methods to assess unconventional reservoirs a case study from the Permian Basin, Texas: WTGS Fall Symposium.

Sen, S., J. Corless, S. Dasgupta, C. Maxwell, and M. Kumar, 2017, Issues faced while calculating overburden gradient and picking shale zones to predict pore pressure: First EAGE Workshop on Pore Pressure Prediction.

Sen, S., A. Kundan, V. Kalpande, and M. Kumar, 2019, The present-day state of tectonic stress in the offshore Kutch-Saurashtra Basin, India: Marine and Petroleum Geology, **102**, 751–758, doi: 10.1016/j.marpetgeo.2019.01.018.

Sen, S., A. Kundan, and M. Kumar, 2018, Post-drill analysis of pore pressure and fracture gradient from well logs and drilling events — An integrated case study of a high pressure exploratory well from Panna East, Mumbai Offshore Basin, India: AAPG Asia Pacific Geosciences Technology Workshop.

Sen, S., A. Kundan, and M. Kumar, 2020, Modeling pore pressure, fracture pressure and collapse pressure gradients in Offshore Panna, Western India: Implications for drilling and wellbore stability: Natural Resources Research, **29**, 2717–2734, doi: 10.1007/s11053-019-09610-5.

Sharma, S. S., P. K. Kulkarni, A. Kumar, P. Pankaj, R. Venkateshwaran, and P. G. H. Susanta, 2010, Successful hydrofracturing leads to opening of new frontiers in shale gas production in the Cambay Basin in Gujarat, India: IADC/SPE Asia Pacific Drilling Technology Conference and Exhibition.

Sharma, V., and A. Sircar, 2018, Demarcating sweet spots in cambay shale by integrating rock eval pyrolysis, geomechanics and seismic data: Abu Dhabi International Petroleum Exhibition and Conference, Paper SPE-193336-MS.

Sharma, V., and A. Sircar, 2019, Mineralogical assemblage of Cambay Shale of North Cambay Basin, Gujarat, India: Journal of Petroleum Exploration and Production Technology, **9**, 87–95, doi: 10.1007/s13202-018-0505-9.

Singh, A., S. K. Das, A. D. Sinha, and P. Singh, 2018, Global shale gas and oil distribution with geological age vis-à-vis Indian Synrift Shale Sequences: ONGC Bulletin, **53**, 149–162.

Sinha, A. K., S. K. Das, S. K. Jha, and Y. R. Chandra, 2018, Shale-oil resource system in Cambay Basin, India: ONGC Bulletin, **53**, 163–180.

Soeder, D. J., 2018, The successful development of gas and oil resources from shales in North America: Journal of Petroleum Science and Engineering, **163**, 399–420, doi: 10.1016/j.petrol.2017.12.084.

Sone, H., and M. D. Zoback, 2013, Mechanical properties of shale-gas reservoir rock — Part 1: Static and dynamic elastic properties and anisotropy: Geophysics, **78**, no. 5, D381–D392, doi: 10.1190/geo2013-0050.1.

Tingay, M., 2015, Initial pore pressures under the Lusi mud volcano, Indonesia: Interpretation, **3**, no. 1, SE33–SE49, doi: 10.1190/INT-2014-0092.1.

Tyagi, A., A. Abedeen, and T. Dutta, 2011, Petrophysical evaluation of shale gas reservoir: A case study from Cambay basin, India: SPE/DGS Saudi Arabia Technical Symposium and Exhibition, SPE 149039.

Verma, S., T. Zhao, K. J. Marfurt, and D. Devegowda, 2016, Estimation of TOC and brittleness volume: Interpretation, **4**, no. 3, T373–T385, doi: 10.1190/INT-2015-0166.1.

Vernik, L., and C. Landis, 1996, Elastic anisotropy of source rocks: Implications for hydrocarbon generation and primary Migration1: AAPG Bulletin, **80**, 531–544, doi: 10.1306/64ED8836-1724-11D7-8645000102C1865D.

Vernik, L., and J. Milovac, 2011, Rock physics of organic shales: The Leading Edge, **30**, 318–323, doi: 10.1190/1.3567263.

Wang, F. P., and J. F. W. Gale, 2009, Screening criteria for shale-gas systems: Gulf Coast Association of Geological Societies Transactions, **59**, 779–793.

Wang, G. -C., M. -Z. Sun, S. -F. Gao, and L. Tang, 2018, The origin, type and hydrocarbon generation potential of organic matter in a marine-continental transitional facies shale succession (Qaidam Basin, China): Scientific Reports, **8**, 6568, doi: 10.1038/s41598-018-25051-1.

Yang, F., S. Xu, F. Hao, B. Hu, B. Zhang, Z. Shu, and S. Long, 2019, Petrophysical characteristics of shales with different lithofacies in Jiaoshiba area, Sichuan Basin, China: Implications for shale gas accumulation mechanism: Marine and Petroleum Geology, **109**, 394–407, doi: 10.1016/j.marpetgeo.2019.06.028.

Biographies and photographs of the authors are not available.